Colloid Polym Sci (2006) 284: 1211–1219
DOI 10.1007/s00396-006-1499-2

ORIGINAL CONTRIBUTION

S. Schleidt
H. W. Spiess
G. Jeschke

A site-directed spin-labeling study of surfactants in polymer–clay nanocomposites

Received: 30 March 2006
Accepted: 11 April 2006
Published online: 4 May 2006

S. Schleidt · H. W. Spiess ·
G. Jeschke (✉)
Max Planck Institute
for Polymer Research,
Postfach 3148,
55021 Mainz, Germany
e-mail: jeschke@mpip-mainz.mpg.de
Tel.: +49-6131-379247
Fax: +49-6131-379100

Abstract Polymer–clay nanocomposites exhibit much improved mechanical, physical, and chemical properties compared to the pure polymer. The interaction of polymer and organically modified silicates is mainly influenced by the surfactant layer in the system. To investigate the structure and dynamics of this surfactant layer, various electron paramagnetic spectroscopy (EPR) techniques were applied. Continuous wave EPR experiments showed a temperature-dependent heterogeneous mobility of the surfactant layer in organoclay as well as a difference in dynamics along the alkyl chain. Intercalation of polystyrene causes a significant slowdown in surfactant dynamics. Electron spin echo envelope modulation indicates a closer contact of the polymer with the mid of the surfactant tail than with the end of the tail. From the obtained data the picture of flatly lying surfactants on clay platelets with a mobility gradient along their alkyl chains can be drawn.

Keywords Polymer–clay nanocomposites · Surfactant layer · Structure · Dynamics · EPR

Introduction

In the last two decades, polymer nanocomposites have moved into the focus of science. As a new class of materials, polymer–clay nanocomposites exhibit much improved properties including mechanical, thermal, gas and liquid barrier, flame retardancy, optical and electrical properties as well as better biodegradability compared to the pure polymer, which make these materials for instance interesting for packaging and automotive industries [1]. As the improved properties can be obtained at low contents of less than 5 wt % of clay, the composites do not lose transparency or gain much weight [2, 3]. The property improvements rely critically on intercalation of the polymer chains between the silicate layers and exfoliation of the silicate platelets. For unpolar polymers like polystyrene, these processes require compatibilization of the clay. The most popular route to achieve this is by ion exchange with surfactants like organic ammonium or phosphonium cations to turn the hydrophilic clay into a hydrophobic component [4]. The dependence of intercalation and exfoliation on the type of surfactant and on processing conditions is not yet understood on a fundamental level. The surfactant layer on the clay affects the entropy and enthalpy of polymer intercalation as well as the interaction of polymer and clay in the nanocomposite and is therefore crucial for the improved properties of the material. Structure and dynamics of the surfactant layer are thus of great interest to optimize design, manufacturing, and applications of polymer–clay nanocomposites [5, 6].

Different techniques have been used in the past to characterize clay-based polymer nanocomposites including rheology for mechanical properties, X-ray diffraction and transmission electron microscopy to gain information about the morphology of the system, as well as thermogravimetric analysis and nuclear magnetic resonance (NMR) to quantify surfactant loading in organoclay [7–9]. Electron paramagnetic spectroscopy (EPR) offers new insight into the surfactant layer of nanocomposites by providing access to structure and in the range of 0.3 to 10 nm and dynamics in the range of 10 ps to 1 μs [10]. Recently, we showed that there are two fractions of

surfactants in organoclay and polymer–clay nanocomposites, which differ in their mobility [11, 12]. We also demonstrated a difference in dynamics between the head group and the tail end of surfactants in the investigated materials. Complete intercalation of polystyrene took place when the organoclay was modified with ammonium-based surfactants while phosphonium-based organoclays lead to no intercalation [12].

In this study, we extend our EPR approach by studying surfactant dynamics and proximity to the polymer chain at different positions along the alkyl chain of the surfactant. The paper is organized as follows: After the syntheses and methods section, we discuss changes in dynamics along the surfactant tail before and after addition of polystyrene. This information can be obtained from continuous wave (CW) EPR spectra. Further investigations with electron spin echo envelope modulation experiments (ESEEM) [13] probe the contact between the spin label on the surfactant with deuterated polymer chains in polymer/layered silicate nanocomposites. With these results, we support and emphasize a structural picture of flatly lying surfactants in organoclay with a mobility gradient along their alkyl chains.

Experimental section

Materials

Synthetic fluoromica Somasif ME-100 with very low content of iron was a gift from Co-Op Chemical, Japan. The surfactant hexadecyltrimethylammonium chloride (HTMA, Aldrich) was used as received. The different spin-labeled surfactants were synthesized as described below. Polystyrene with a narrow molecular weight distribution (GPC standard, PS10k, M_w ~9,500, M_w/M_n ~1.06, T_g=370 K) was obtained from Fluka. Anionically polymerized perdeuterated polystyrene (PS10k-d8, M_w ~10,950, M_w/M_n ~1.04) was obtained from Polymer Laboratories.

Synthesis of surfactant spin-labeled at the end of its alkyl chain

2-(11-Bromo-undecyl)-isoindole-1,3-dione

11-Bromoundecanol (Fluka, 5.02 g) and potassium phtalimide (Fluka, 3.70 g) were reacted for 5 h in DMF (20 ml) at 80 °C. After cooling down, the reaction mixture was dissolved in chloroform (40 ml) and extracted two times with water (70 ml). The water phases were extracted two times with chloroform (20 ml). The combined organic phases were washed first with 0.2 M NaOH (20 ml) and then with water (20 ml). The solution was dried (Na_2SO_4). The solvent was removed in vacuo, and 2-(11-hydroxy-undecyl)-isoindole-1,3-dione (1a) was obtained as a colorless solid (5.58 g, 88 %). Tetrabromomethane (Fluka, 3.13 g), triphenylphosphine (Aldrich, 2.48 g), and 1a (2.00 g) were stirred overnight in diethylether (60 ml) at room temperature. Filtration over silica gel with petroleum ether/acetone (5:1) as a solvent made 2-(11-bromo-undecyl)-isoindole-1,3-dione (1,72 g, 72 %) as a pale yellow solid.

Quaternization

To a solution of 2-(11-bromo-undecyl)-isoindole-1,3-dione (1.53 g) in ethanol (55 ml), an aqueous solution of trimethylamine (Fluka, 45–50 %, 8.2 ml) was added. After stirring for 7 days at room temperature and removing the solvent and excess of trimethylamine at 45 °C and a pressure of 110–120 mbar, the yellow, solid residue was dissolved in ethanol (30 ml) and precipitated using diethylether (120 ml) to make trimethyl-[11-(1,3-dioxo-1,3-dihydro-isoindol-2-yl)-undecyl]-ammonium bromide (1b) a pale yellow solid (1.29 g, 75 %).

Deprotection and spin labeling

An aqueous solution of hydrazine hydrate (Fluka, 25 %, 1.17 ml), methanol (60 ml), and 1b (1.29 g) were refluxed for 1 h. After addition of water and evaporation of methanol, concentrated hydrochloric acid was added and the mixture was further refluxed for 1 h. After cooling down, a white precipitate was removed and the clear yellow solution was extracted two times with ethyl acetate (30 ml). The aqueous phase was concentrated to dryness, and (11-amino-undecyl)-trimethyl-ammonium bromide as yellow solid (1b, 0.53 g, 58 %) was obtained. For spin-labeling, to a solution of 1b (0.27 g) in dry THF (15 ml) were added 2,2,5,5-tetramethyl-3-pyrroline-1-oxyl-3-carboxylic acid (Aldrich, 0.24 g) and DMAP (Merck, 0.18 g). DCC (Fluka, 0.27 g) was added under ice cooling, and the mixture was then stirred for 3 days at room temperature. After separating from the precipitated urea to the clear yellow solution, 2 M HCl (40 ml) was added. The mixture was extracted two times with diethylether (20 ml), the combined organic phases were dried (Na_2SO_4), and the solvent was removed in vacuo. Compound 1 was obtained as yellow solid (0.38 g, 91 %). Identity of the compounds was checked by mass spectroscopy, and ^{1}H- and ^{13}C-NMR and for paramagnetic substances by IR spectroscopy.

General route for the synthesis of surfactant spin-labeled at a defined position along its alkyl chain

10-Bromo-2-ethyldecane acid

Sodium (Aldrich, 2.30 g) was dissolved in ethanol (100 ml) under gradual heating. The warm solution was added dropwise to ethylmalonic acid diethylester (Aldrich, 18.82 ml) and 1,8-dibromooctane (Aldrich, 27.94 ml), and the mixture was stirred for 4 h at 90 °C and overnight at room temperature. After evaporation of the solvent and addition of water, the organic phase was separated and extracted two times with diethylether (50 ml). The combined organic phases were dried (Na_2SO_4), and the solvent was removed in vacuo. After vacuum distillation, 2-(8-bromooctyl)-2-ethylmalonic acid diethylester (2a) was obtained as yellow oil (24.97 g, 66 %). Potassium hydroxide (WTL Laborbedarf, 11.37 g) and 2a were dissolved in a mixture of water (14 ml) and ethanol (28 ml) and refluxed for 16 h; the solvent was then removed in vacuo. The residue was dissolved in water, and concentrated hydrochloric acid was added under ice cooling to adjust the pH value to 1. The mixture was then extracted four times with diethylether (50 ml). The combined organic phases were washed with brine (30 ml) and then dried ($MgSO_4$), and the solvent was removed in vacuo to obtain crude 2-(8-bromooctyl)-2-ethylmalonic acid (2b) as yellow, highly viscous liquid (16.27 g, 87 %). Heating followed by vacuum distillation of 2b (16.00 g) yields 10-bromo-2-ethyldecane acid as a yellow oil (11.88 g, 86 %).

Quaternization

To a solution of 10-bromo-2-ethyldecane acid (4.29 g) in ethanol (150 ml), an aqueous solution of trimethylamine (Fluka, 45–50 %, 30 ml) was added. After stirring for 7 days at room temperature and removing the solvent and excess of trimethylamine at 65–70 °C and a pressure of 50–60 mbar, (9-carboxyundecyl)-trimethyl ammonium bromide (2c) was obtained as a yellow, highly viscous liquid (4.83 g, 93 %).

Spin-labeling

To a solution of 2c (1.52 g) in dry THF (20 ml) were added 4-amino-2,2,6,6-tetramethylpiperidin-1-oxyl (Aldrich, 1.00 g) and DMAP (Merck, 1.82 g). Then, DCC (Fluka, 2.77 g) was added under ice cooling, and the mixture was stirred for 3 days at room temperature. After separating from the precipitated urea to the clear yellow solution, 2 M HCl (40 ml) was added. The mixture was extracted three times with diethylether (40 ml), the combined organic phases were dried (Na_2SO_4), and the solvent was removed in vacuo. Compound 2 was obtained as red oil (1.94 g, 88 %). In the analogous manner, compound 3 was obtained as red oil (1.91 g, 86 %). Identity of the compounds was checked by mass spectroscopy, and ^{1}H- and ^{13}C-NMR and for paramagnetic substances by IR spectroscopy. Phosphonium-based surfactants were synthesized in an analogous way.

Preparation of organoclay

To a dispersion prepared by stirring 2 g of Somasif ME-100 in 200 ml of deionized water for about 30 min was added a solution of the appropriate amount of HTMA and of spin probes in a mixture of 40 ml of deionized water and 40 ml of ethanol that was kept at 60 °C. This corresponds to surfactant excess samples with a threefold excess of HTMA with respect to the cation exchange capacity (CEC: 0.85 meq/g) of Somasif ME-100. The amount of spin probes used (1: 20 mg, 2: 15 mg, and 3: 15 mg) ensured that less than 2 % of foreign surfactant molecules were introduced. No spectral broadening due to dipole–dipole interaction between electron spins was observed. Furthermore, the required space of the used nitroxide spin label was small enough not to disturb the structure of the investigated systems. After stirring the combined solutions at 60 °C for 5 h, the precipitate was collected by filtration and washed with a 1:1 hot mixture of deionized water and ethanol until an $AgNO_3$ test for chloride ions in the washing liquid was negative. The obtained material was dried in the vacuum oven at 70 °C for 24 h. EPR samples were prepared by pressing 100 mg of organoclay at a temperature of 433 K for 30 min at 70 MPa in a Weber-Press (Maschinen Apparatebau GmbH).

Preparation of nanocomposites

Mixtures of 75 mg polymer and 25 mg organoclay were pressed at temperatures of 433 K for 30 min at 70 MPa in a Weber-Press.

EPR measurements

Spectra were recorded on a Bruker ELEXSYS 580 EPR spectrometer at X-band frequencies (9.3–9.8 GHz). Variable temperature CW EPR was performed with a 4103 TM resonator using a glass dewar and the Bruker ER 4111 VT temperature control unit. Extrema separations $2A_{zz}$ for completely immobilized nitroxides were measured at a temperature of 80 K. A microwave power of 2 mW, modulation amplitude of 0.1 mT, and a modulation frequency of 100 kHz were employed. Three-pulse ESEEM experiments [13] were performed at a temperature of 50 K and at the maximum of the nitroxide spectrum using a Bruker Flexline split-ring resonator ER 4118X_MS3. Pulse widths were 16 ns, and the interpulse

delay between the first two pulses was 344 ns to obtain a favorable ratio of deuterium to proton modulations. An increment of 16 ns was used for the second interpulse delay, and 1,024 data points were acquired.

Results

In previous papers, we applied commercial head group-labeled and a homemade end-labeled surfactants (1 and analogous tributylphosphonium-based surfactants) to obtain first insight into the structure and dynamics of the surfactant layer [11, 12]. For further elucidation of the microstructure of the surfactant layer in organically modified clay and polymer–clay nanocomposites, surfactants spin-labeled at specific sites along the surfactant tail were synthesized as described above. The molecular structures of the specifically synthesized, spin-labeled surfactants are presented in Fig. 1. Characterization of samples containing 1, 2, and 3 should result in a more detailed structural picture of the investigated materials.

The CW EPR spectrum of nitroxide spin labels is dominated by a triplet splitting. The maximum extrema separation $2A'_{zz}$ (Figs. 2 and 4a) of the spectral lineshape is the difference of the resonance fields of the low-field maximum to the high-field minimum of the spectrum. If the extrema separation $2A_{zz}$ for the completely immobilized nitroxide is known, $2A'_{zz}$ can be analyzed in terms of the rotational correlation time τ_r of the spin label in the range between 10 ps and 1 μs (Fig. 2) [14–16]. If the

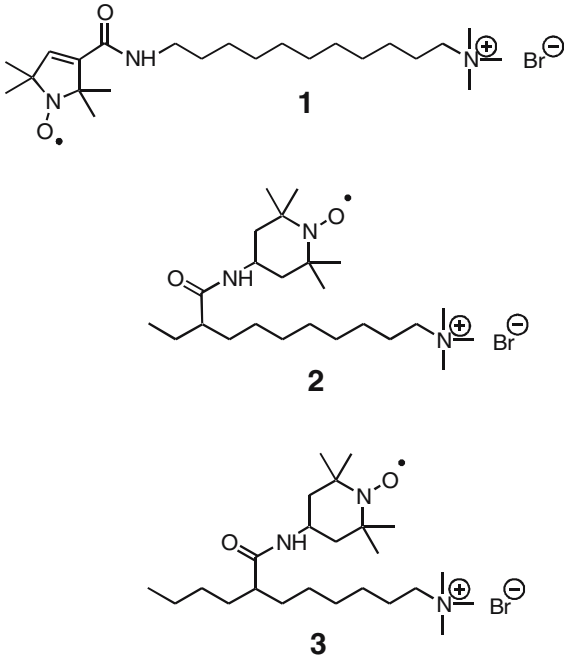

Fig. 1 Molecular structures of the specifically synthesized, spin-labeled surfactants 1, 2, and 3 carrying a nitroxide spin label at defined positions along their alkyl chains

dynamics of the spin label is fast on the CW EPR time scale (τ_r<10 ps), the resulting spectrum shows a simple triplet pattern with uniform line widths. In the range 10 ps<τ_r<3 ns, the line widths differ, but the spectrum is still a simple triplet. For correlation times τ_r>3.5 ns, dynamics is slow on the EPR time scale, and the spectral lineshape becomes more complicated. Finally, for τ_r>1 μs, a powder pattern results. The most distinctive changes in the spectral lineshape can be observed within one decade between 1 and 10 ns. In accordance, dramatic changes of the spectral lineshape are expected only in a narrow temperature range.

In contrast to the simulated spectra in Fig. 2, all measured CW EPR spectra show heterogeneous dynamics within the surfactant layer (slow and fast components), like e.g., Fig. 3a showing end-labeled tributylphosphonium-based surfactant analogous to 1. To get an idea about the different τ_r in the investigated samples, computer-simulated spectra of slow and fast components with known τ_r were superimposed. Figure 3b shows such bimodal spectra where the τ_r of the components (ratio 1:1) differ by one decade. Among the simulated spectra, spectrum iii is most sensitive to dynamic heterogeneities. Here, τ_r is 10 ns for the slow component and 1 ns for the fast component. To illustrate the effect of varying the fractions of slow and fast components in the samples, Fig. 3c shows mixed spectra of both components in different ratio with τ_r of 10 and 1 ns. Note that the spectrum with ratio 20:80 (bottom trace) closely resembles the spectrum at 353 K (top trace) in Fig. 3a. Thus, by comparing experimental spectra to such simulations, a semiquantitative analysis of slow and fast components in the investigated materials can be made.

The CW EPR spectra in Fig. 4 show the increasing mobility of the surfactant layer in organically modified clay with increasing temperature. Presented are organoclay samples I, II, and III containing 1 % of specifically synthesized, spin-labeled surfactant 1, 2, or 3. By comparison to Fig. 3c, it can be estimated that at room temperature, the fraction of the slow component in I is about 80 %; at 333 K, this number decreases to about 20% (Fig. 4a). For II and III, the fractions of the slow component at the same temperatures are significantly higher (Fig. 4b,c). Furthermore, these CW EPR experiments show the existence of a dynamic gradient within the surfactant layer. Moving the spin label from the surfactant chain end (1) towards the mid of the chain (3), the mobility of the fast fraction decreases. Together with the results from former experiments using head-labeled surfactants [11, 12], these results indicate that the head groups of the surfactants are largely immobilized at the clay surface while the chain ends remain mobile.

After addition of polystyrene, the increase in mobility of the surfactants is generally observed at higher temperatures (Fig. 5). Polymer—intercalated or not—reduces the volume in which the surfactant chains can move. Below the glass transition temperature of the polymer, the platelets cannot change their basal spacing, thus the polymer dominates the dynamics of the system. After reaching the

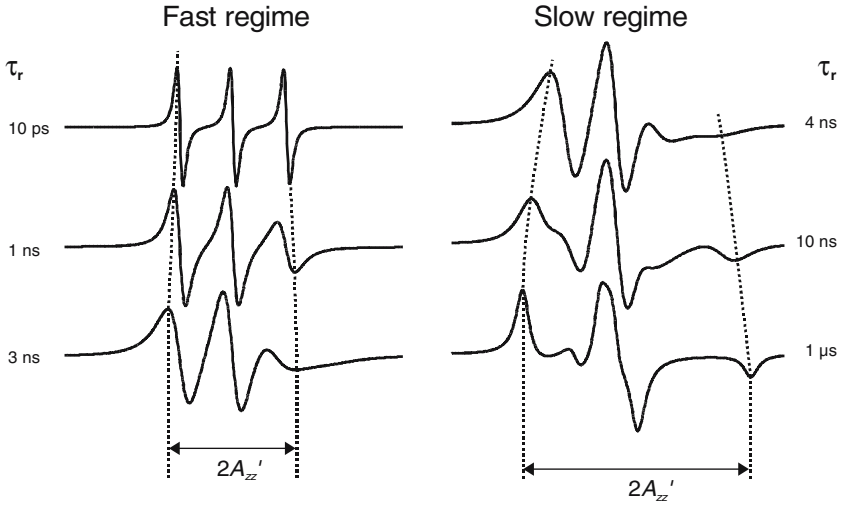

Fig. 2 Simulated spectra of a nitroxide spin label showing the variation of the lineshape and of the maximum extrema separation $2A'_{zz}$ with varying rotational correlation time τ_r

glass transition temperature of the polystyrene, the mobility of the system approaches the dynamics of the pure organoclay. For comparison of different positions along the surfactant chain, consider the CW EPR spectra of polymer–clay nanocomposites I-PS, II-PS, and III-PS each containing 1 % of the spin-labeled surfactant 1, 2, or 3 shown in Fig. 5. While in I at higher temperatures just a fast component can be detected (Fig. 4a), a slow component with a content of roughly 60 % can be observed in I-PS even at 353 K (Fig. 5a). Addition of polystyrene to II and III also results in a general slowdown of surfactant dynamics. In contrast to II, where a fast component is observable, in II-PS, the fraction of the slow component is always near 100 % (Fig. 5b). A fast component is not detectable. The situation is similar for III-PS (Fig. 5c), although the slowdown is less pronounced in this case.

As in organoclay also in polymer–clay nanocomposites, a dynamic gradient within the surfactant layer can be observed. Addition of polymer generally restricts the mobility of the surfactant layer. In other words, the dynamics of the system is dominated by the mobility of the surrounding polymer matrix. The direct comparison of the dynamics in sample II without and with polymer is illustrated in Fig. 6a showing the maximum extrema separation of the spectral lineshape $2A'_{zz}$ (for definition, see Figs. 2 and 4a) plotted against temperature. It can clearly be seen that with increasing temperature, the mobility of the sample without polymer (empty triangles) increases, i.e., $2A'_{zz}$ decreases, already slightly above 300 K. In contrast, in II-PS with polymer (full circles), a fast component with a small $2A'_{zz}$ is observable only above 400 K. In contrast to this intercalated nanocomposite, Fig. 6b shows the analogous sample with tributylphosphonium-based surfactant, where no intercalation of polymer took place and only a microcomposite was formed [12, 17]. Again, the dynamics in the pure organoclay (empty

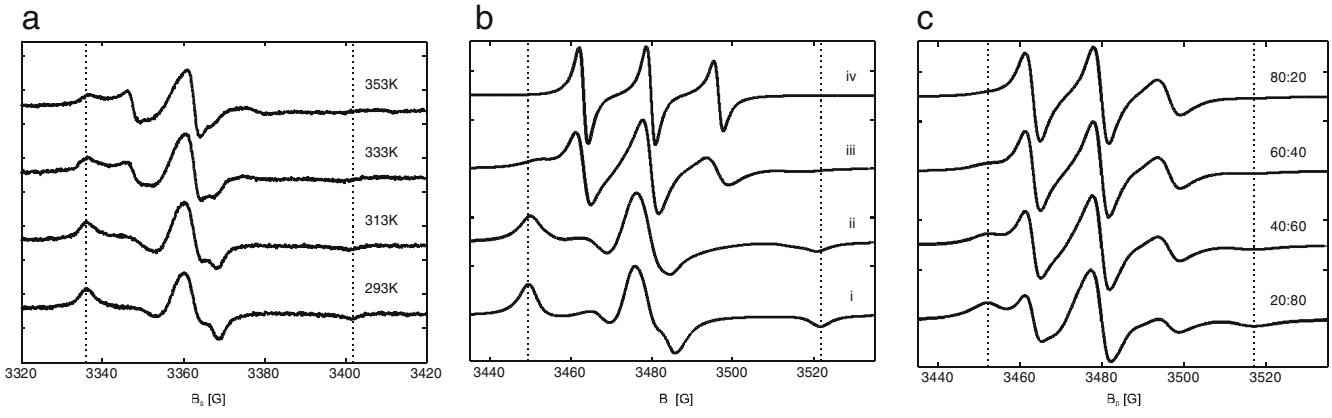

Fig. 3 Dynamic heterogeneity in organoclays and polymer–clay nanocomposites. The *vertical dotted lines* denote the extrema of the slow component. **a** Experimental CW EPR spectra of an organoclay containing end-labeled, tributylphosphonium-based surfactants. **b** Computer-simulated spectra comprising a slow and a fast component (ratio 1:1) with rotational correlation times τ_r differing by one decade. i: $\tau_{r,\ slow}$=1 µs, $\tau_{r,\ fast}$=100 ns; ii: $\tau_{r,\ slow}$=100 ns, $\tau_{r,\ fast}$=10 ns; iii: $\tau_{r,\ slow}$=10 ns, $\tau_{r,\ fast}$=1 ns; iv: $\tau_{r,\ slow}$=1 ns, $\tau_{r,\ fast}$=0.1 ns. **c** Computer-simulated spectra of components with rotational correlation times of 10 ns for the slow and 1 ns for the fast component in diverse ratios (*shown right*)

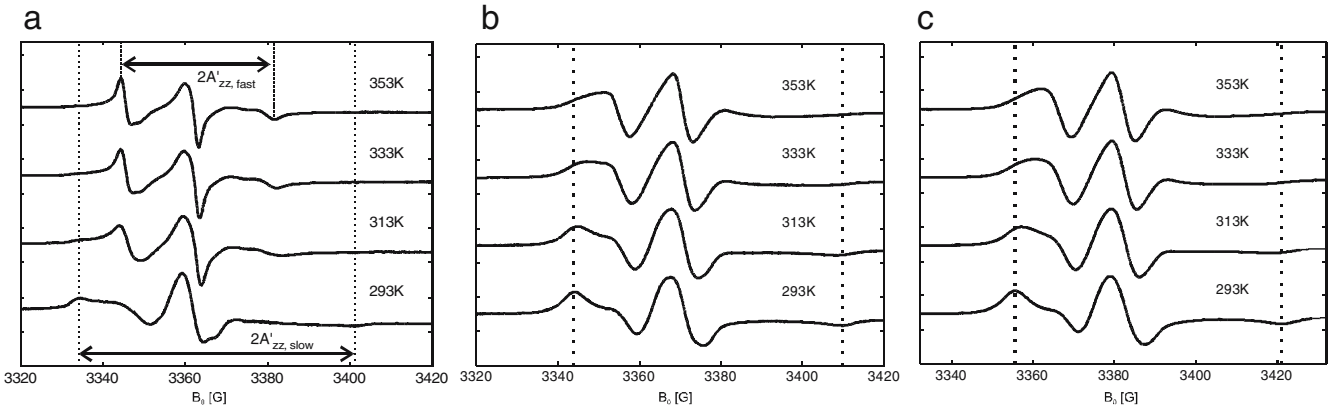

Fig. 4 CW EPR spectra of samples I, II, and III each containing 1 % of specifically synthesized, spin-labeled surfactant 1 (**a**), 2 (**b**), or 3 (**c**). Moving the spin label from the alkyl chain end toward its middle results in spectra showing lower mobility. The *vertical dotted lines* denote the extrema of the slow component

triangles) is higher than the one in the composite (full circles), but in comparison to II-PS, the surfactant layer in the polymer sample with tributylphosphonium-based surfactants demonstrates a higher mobility and a more gradual melting of the surfactant layer already below the glass transition temperature of polystyrene. Thus, intercalated polymer seems to restrict the dynamics of the system more strongly than a polymer matrix that only surrounds the stacks of organoclay platelets.

With ESEEM, it is possible to probe the contact between spin label and deuterated polymer. The deuterium in the polymer creates a contrast to the protons in the surfactant and clay, so that the signals can be clearly assigned to the polymer. We have checked by both WAXS and CW EPR that deuteration of polystyrene does not influence structure or dynamics of the composites. ESEEM experiments on sample I-PS-d8, II-PS-d8, and III-PS-d8 containing deuterated polystyrene show that the contact between polymer and mid of the surfactant tail is somewhat closer than the one between polymer and end of tail. Figure 7a presents the original ESEEM data showing different modulation depth for the investigated polymer–clay nanocomposites. It can be seen that the contact—represented by the modulation depth—between polymer and end of surfactant tail in I-PS-d8 is not as close as between polymer and mid of surfactant tail in II-PS-d8 and III-PS-d8. This is even more obvious in the spectral representation shown in Fig. 7b, where the deuterium signal at 2 MHz in I-PS-d8 is weaker than in II-PS-d8 and III-PS-d8.

Analysis of the modulation depth gives information about the number of deuterium nuclei in contact to the spin label and their distance [18–20]. In sample I-PS-d8, the smallest distance is about 0.35 nm and the average number of spin label in contact to polystyrene is 0.26, which means that about one in four paramagnetic centers is in contact to polymer. Samples II-PS-d8 and III-PS-d8 are similar to each other. In both cases, the distance between spin label and polymer is 0.37 nm and the average number of spin labels in contact to polymer is 0.38 and 0.37, respectively.

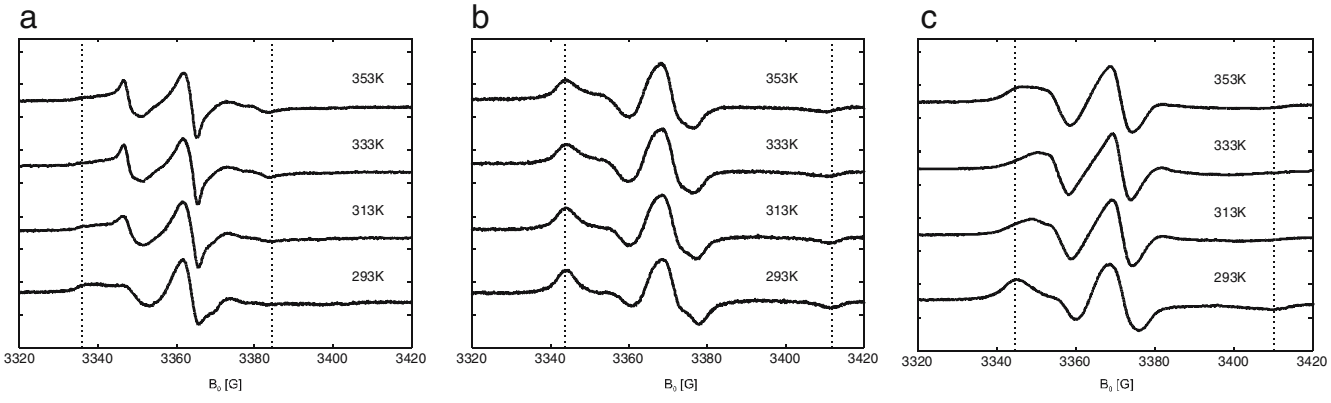

Fig. 5 CW EPR spectra of polymer–clay nanocomposites I-PS (**a**), II-PS (**b**), and III-PS (**c**) each containing 1 % of specifically synthesized, spin-labeled surfactant 1 (**a**), 2 (**b**), or 3 (**c**). Addition of polymer restricts the mobility of the surfactant layer. The *vertical dotted lines* denote the extrema of the slow component

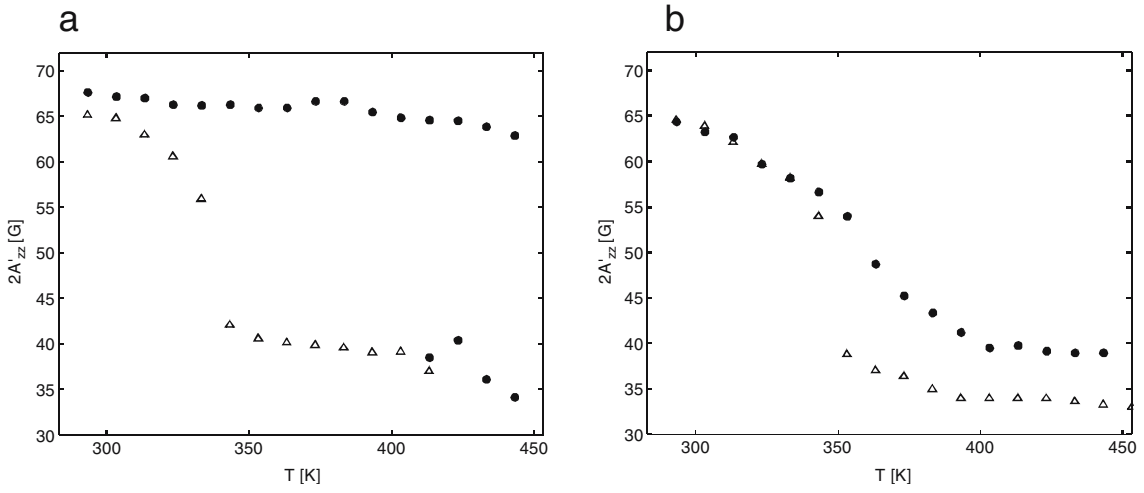

Fig. 6 Dependence of the maximum line splitting $2A'_{zz}$ on temperature. A decrease of $2A'_{zz}$ corresponds to an increase in mobility. **a** Sample II (*empty triangles*) and II-PS nanocomposite (*full circles*). **b** Tributylphosphonium analogon of sample II (*empty triangles*) and its microcomposite with polystyrene (*full circles*)

This corresponds to more than one in three centers in contact to the polymer chains.

Discussion

Former NMR [12] and gravimetric [21] measurements as well as simulations [6] predict a surfactant multilayer system in organoclay when using an excess of surfactant with respect to the CEC of the clay. Due to electrostatic interactions, one fraction of surfactants is localized directly on the clay surface building a bilayer between the platelets. The other surfactant fraction is located in between this bilayer thus creating a multilayer. This picture is supported by our CW EPR experiments where slow and fast components can be detected. The slow component corresponds to the fraction localized on the clay surface, while the fast component to the fraction in between these surface layers. With increasing temperature, the surfactant layer melts gradually, the platelets expand, the clay swells, and the dynamics of the system raises, which means that $2A'_{zz}$ as the maximum splitting of the spectral lineshape is getting smaller.

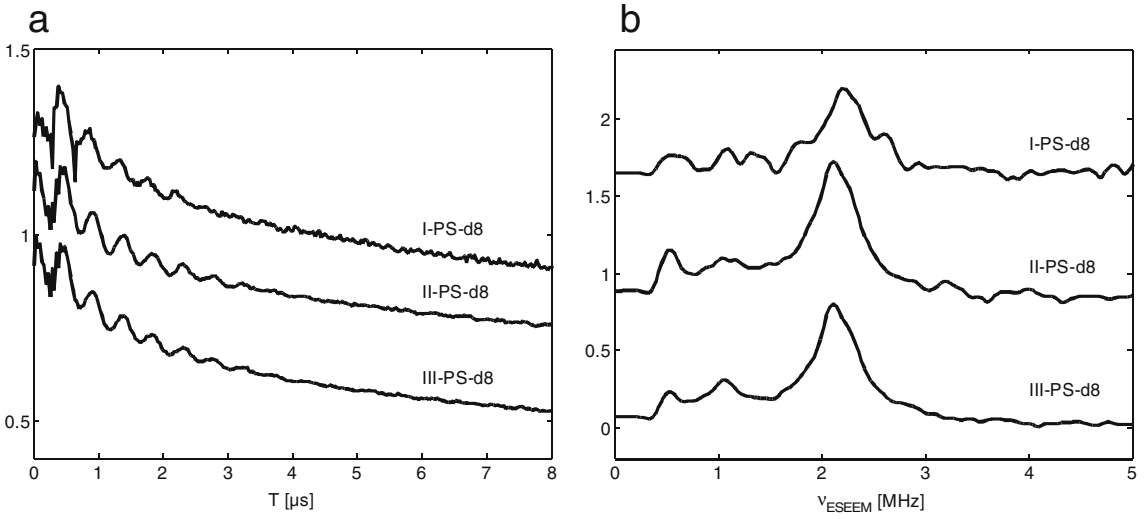

Fig. 7 Characterization of surfactant-polymer contacts by ESEEM. **a** Original ESEEM data showing different modulation depth for polymer–clay nanocomposites I-PS-d8, II-PS-d8, and III-PS-d8 based on fully deuterated polystyrene and each containing 1 % of specifically synthesized, spin-labeled surfactant 1 (I), 2 (II), or 3 (III). **b** Corresponding ESEEM spectra showing a deuterium signal at 2 MHz indicating contact between polymer and surfactant tail. The closest contact with the strongest signal can be seen for samples containing 2 and 3

The actual molecular structure of the surfactant layer in organoclay was studied before by Fourier transform infrared (FTIR) spectroscopy [22]. This method is sensitive to the ratio of *gauche*/*trans* conformations in alkyl chains by observing frequency and width of the asymmetric CH_2 stretching vibrations. FTIR experiments showed that there also exists a significant fraction of *gauche* conformation within the surfactant layer. This liquid-like fraction diminishes with increasing surfactant concentration. The same observation was made in a Raman study [23]. A quantitative analysis of the *gauche*/*trans* ratio was performed by a solid-state NMR technique [24]. For a montmorillonite modified with 1-octyldecylamine, about 67 % of the alkyl chains are in an all-*trans* conformation at room temperature. With increasing temperature, disorder increases and the surfactant layer in organoclay exhibits a more liquid–crystalline character. Melting of the surfactant layer takes place over a broad temperature range as observed experimentally [12] and predicted earlier by simulations of molecular dynamics (MD) for alkyl chains tethered to a silica surface [25]. MD simulations also provide the ratio of *gauche*/*trans* conformations in surfactant alkyl chains in a multilayer organoclay system [26], and they propose that the order of the surfactant alkyl chains decreases with increasing distance from the head group [27].

There already exist some suggestions for the nanostructure of the surfactant layer in organoclay. They are derived from model-based analysis of X-ray diffraction experiments [28] and MD simulations [6] and propose that in organically modified clay, the surfactant head groups are anchored on the clay surface and the surfactant tails are almost parallel to it. Our ESEEM experiments support this picture and provide new insight into the structure of such systems. They demonstrate that in our composites besides the surfactant head groups [12], also the surfactant tails are in fairly close contact with the polymer chains. Somewhat surprisingly, the contact between polymer and mid of the surfactant tail is closer than the one between polymer and end of tail. This might be explained by the structure of the surfactants. As the nitroxide spin label is attached over a rigid amide bond, it cannot move freely, so its mobility is dominated by the mobility of the surfactant alkyl chain. With the picture of flatly lying surfactants, one can imagine that a nitroxide label attached at the end of the surfactant tail as the most mobile part of the alkyl chain can integrate better in the surfactant layer than a spin label attached somewhere in the middle of the alkyl chain. Together with the CW EPR results, also the ESEEM measurements support the picture of flatly lying surfactants on the clay surface with a dynamic gradient along their alkyl chains (Fig. 8).

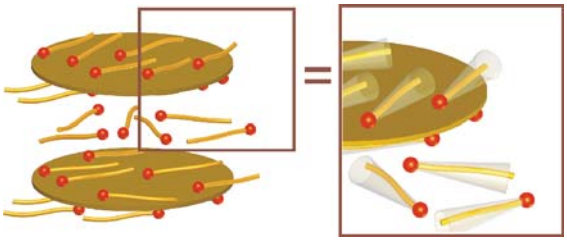

Fig. 8 Structure scheme for organically modified clay. The slow fraction of surfactants is anchored on the clay surface while the more mobile, fast fraction is located between these surface layers. The surfactant tails are almost parallel to the clay surface and exhibit a dynamic gradient along the alkyl chain

Conclusions

EPR spectroscopy provides new insight into the structure and dynamics of the surfactant layer in organoclay and polymer–clay nanocomposites. CW EPR experiments on spin-labeled surfactants provide information on gradual dynamical changes in the investigated materials when increasing the temperature. Heterogeneous dynamics and a dynamic gradient along the surfactant alkyl chain can be observed, whereas the mobility is highest at the chain end. After addition of polystyrene, a decrease in dynamics can be observed, and the mobility of the system is dominated by the mobility of the surrounding polymer matrix. Plotting the extrema separation $2A'_{zz}$ against the temperature, we could distinguish between nano- and microcomposites. ESEEM experiments probe the contact between polymer and nitroxide spin label along the surfactant tail. The measurements indicate a closer contact of polystyrene with the mid of the surfactant tail than with the end of it. The results of both EPR techniques support and emphasize already existing models of the structure in organoclay and polymer–clay nanocomposites, where the surfactants lie flatly on the surface of the clay platelets with a mobility gradient along their alkyl chains.

Thus, EPR spectroscopy can contribute to a better understanding of the relation between structure and dynamics in organoclay and polymer–clay nanocomposites. EPR, NMR, and WAXS experiments with different clays and polymers are in progress to obtain a more general picture of the relations and interactions in these materials.

Acknowledgement We are grateful to Christian Bauer for the technical support.

References

1. Zeng QH, Yu AB, Lu GQ, Paul DR (2005) J Nanosci Nanotechnol 5:1574
2. Ray SS, Okamoto M (2003) Prog Polym Sci 28:1539
3. Balazs AC, Singh C, Zhulina E, Lyatskaya Y (1999) Acc Chem Res 32:651
4. Vaia RA, Teukolsky RK, Giannelis EP (1994) Chem Mater 6:1017
5. Krishnamoorti R, Vaia RA, Giannelis EP (1996) Chem Mater 8:1728
6. Zeng QH, Yu AB, Lu GQ, Standish RK (2003) Chem Mater 15:4732
7. Jordan J, Jacob KI, Tannenbaum R, Sharaf MA, Jasiuk I (2005) Mater Sci Eng A 393:1
8. Jeon HS, Rameshwaram JK, Kim G, Weinkauf DH (2003) Polymer 44:5749
9. Krishnamoorti R, Vaia RA (2001) Polymer nanocomposites: synthesis, characterization, and modeling. American Chemical Society, New York
10. Jeschke G (2004) Electron paramagnetic resonance spectroscopy. In: Steed J, Atwood J (eds) Encyclopedia of supramolecular chemistry. Taylor & Francis, New York, pp 520–527
11. Jeschke G, Panek G, Schleidt S, Jonas U (2004) Polym Eng Sci 44:1112
12. Panek G, Schleidt S, Mao Q, Wolkenhauer M, Spiess HW, Jeschke G (2006) Macromolecules 39:2191
13. Schweiger A, Jeschke G (2001) Principle of pulse electron paramagnetic resonance. Oxford University Press, Oxford
14. Freed JH (1976) Theory of slow tumbling ESR spectra for nitroxides. In: Berliner LJ (ed) Spin labeling—theory and applications, vol 1. Academic, New York, pp 53–132
15. Schneider DJ, Freed JH (1989) Calculating slow motional magnetic resonance spectra: a users's guide. In: Berliner LJ, Reuben J (eds) Biological magnetic resonance, vol 18. Plenum, New York, pp 1–76
16. Berliner LJ (1998) Biological magnetic resonance, vol 14. Plenum, New York
17. Schleidt S (2006) EPR-Spektroskopie zur Untersuchung von Struktur und Dynamik in Polymer-Ton-Nanokompositen. Dissertation, Mainz
18. Ichikawa T, Kevan L, Bowman MK, Dikanov SA, Tsvetkov YD (1979) J Chem Phys 71:1167
19. Hinderberger D (2004) Polyelectrolytes and their counterions studied by EPR spectroscopy. Dissertation, Mainz
20. Hinderberger D, Spiess HW, Jeschke G (2004) J Phys Chem B 108:3698
21. Mao Q (2004) Intermolecular interactions in surfactant layers on clay nanoplatelets. Master Thesis, Mainz
22. Vaia RA, Teukolsky RK, Giannelis EP (1994) Chem Mater 6:1017
23. He HP, Frost RL, Xi YF, Zhu XJ (2004) J Raman Spectrosc 35:316
24. Wang LQ, Liu J, Exarhos J, Flanagan KY, Bordia R (2000) J Phys Chem B 104:2810
25. Klatte SJ, Beck TL (1993) J Phys Chem 97:5727
26. Hackett E, Manias E, Giannelis EP (1998) J Chem Phys 108:7410
27. He HP, Galy J, Gerard JF (2005) J Phys Chem B 109:13301
28. Yang JH, Han YS, Choy JH, Tateyama H (2001) J Mater Chem 11:1305